# AN ANALYSIS OF THE SPALLATION OF CARBON PHENOLIC ABLATORS

---

By

Brian J. O'Hare

Thesis submitted to the Graduate Faculty of the
Virginia Polytechnic Institute
in candidacy for the degree of

MASTER OF SCIENCE

in

AEROSPACE ENGINEERING

---

June 1967

# AN ANALYSIS OF THE SPALLATION OF CARBON PHENOLIC ABLATORS

by

Brian J. O'Hare

Thesis submitted to the Graduate Faculty of the

Virginia Polytechnic Institute

in candidacy for the degree of

MASTER OF SCIENCE

in

AEROSPACE ENGINEERING

APPROVED: _____

_____ _____

_____

June 1967

Blacksburg, Virginia

## II. TABLE OF CONTENTS

## III. LIST OF FIGURES AND TABLES

## IV. INTRODUCTION

The development to date of ablating heat shield materials has made it possible for vehicles to reenter the earth's atmosphere at speeds up to 36,000 feet per second. In the not too distant future, heat shields capable of withstanding the heat loads generated at speeds corresponding to return from an interplanetary mission (up to 50,000 feet per second) will be required. Since the heating rates increase dramatically as speed is increased from 36,000 to 50,000 feet per second, (according to ref. 1, for $V < 36{,}000$ ft/sec, $\dot{q}_{TOT} \propto V^{3.15}$, for $36{,}000 < V < 50{,}000$ ft/sec, $\dot{q}_{TOT} \propto V^{15.45}$) an interplanetary return vehicle will require a highly efficient thermal protection system in order to confine the heat shield weight to a manageable level (i.e. less than approximately 35 percent of total reentry weight).

The carbon phenolic materials, probably the most promising ablation materials in existence today, have a demonstrated ability to form and retain a high strength, high temperature char layer. The char layer, by virtue of its ability to withstand temperature in the neighborhood of $5000^{\circ}$ R or more, contributes to the efficiency of the heat shield by: (1) reradiating heat at rates up to 1000 Btu/ft$^2$-sec, (2) lowering the convective heat input by reducing the temperature difference across the boundary layer $\left(\text{i.e. } T_{aw} - T_w\right)$, (3) reducing the heat conducted to the virgin ablator by virtue of its low thermal conductivity, and (4) in extreme temperature applications by subliming and thereby absorbing additional heat. Thus, char layer integrity is the key to a high performance thermal protection material.

Although the carbon phenolic materials exhibit char retention properties which are superior to those of other materials, they suffer from a serious problem of spallation. Spallation is a process by which large pieces of char "pop off" the heat shield in an apparently random fashion. When spallation occurs it reduces the efficiency of the ablator and large mass losses are incurred. The purpose of this thesis is to obtain a better insight into the nature and causes of the spallation phenomenon and to suggest a technique to substantially reduce the level of spallation.

## V. LITERATURE REVIEW

The phenomenon of spallation in charring ablators is a topic on which surprisingly little has been written. Aside from the analysis presented by Scala and Gilbert (ref. 5) the principal analysis is that of Mathieu[1]. This thesis differs from the first mentioned analysis principally in that the author rejects the form of the momentum equation used by Scala and Gilbert. The reasons for this are given in the text, but it is worthwhile to note here that the internal pressure distribution which Scala and Gilbert obtain has a maximum at some point in the char. Physically, this means that the flow model they postulate requires pyrolysis gases to travel against a pressure gradient until the maximum pressure location is reached. Since the gases have a negligibly small initial velocity, this flow model does not appear consistent with reality. This contrasts with the result obtained in this thesis, namely a favorable pressure gradient at every point in the char.

Mathieu, although apparently using the proper form of the momentum equation, concerns himself primarily with a shear removal mechanism (it is to be noted that carbon phenolic ablators form strong chars which are highly shear resistant).

In neither of the above mentioned analyses is the permeability considered to be as low as the values measured and reported herein.

---

[1]Mathieu, R. D.; Theoretical Analysis for the Mechanical Spallation of a Typical Charring Ablator During Reentry. R63SD53 General Electric Missile and Space Division, Dec. 1963.

In addition, neither author considers the effect of a varying permeability.

Finally, it should be noted that the literature does contain a hypothesis not yet mentioned. This hypothesis[2] states that as pyrolysis gases flow through the hot char, they crack and deposit carbon on the char skeleton. This deposition of carbon causes a blockage of flow and a consequent spallation. To the author's best knowledge, this "cracking" hypothesis has yet to be proven. The present analysis suggests that, rather than by cracking of hydrocarbons, the permeability reduction occurs by a process of solid particle entrapment. This explanation appears the more logical to anyone who has worked with charred ablators and has seen the copious amounts of "coal dust" which are characteristic of these materials.

---

[2] Robbins, D. L.; Thermal Erosion of Ablative Materials, ASD-TR-61-307, Aerojet General Corp., 1962.

## VI. LIST OF SYMBOLS

| | |
|---|---|
| $A$ | frequency factor, 1/sec |
| $C_p$ | specific heat at constant pressure, $Btu/lb_m$ |
| $\Delta E$ | activation energy, cal/mol |
| $\vec{g}$ | local gravity vector, $ft/sec^2$ |
| $g_o$ | reference gravitational constant, $ft/sec^2$ |
| $H^*$ | parameter defined in equation 14 |
| $H_p$ | heat of pyrolysis, $Btu/lb_m$ |
| $k$ | permeability, $ft^2$ |
| $K$ | thermal conductivity, $Btu/ft^2\text{-}sec\text{-}^oR/ft$ |
| $\dot{m}_g$ | mass flow rate per unit area, $lb_m/ft^2\text{-}sec$ |
| $\bar{M}$ | molecular weight, $lb_m/lb\ mol$ |
| $n$ | experimentally determined exponent in (equation (8)) |
| $p$ | porosity |
| $P$ | pressure, $lb_f/ft^2$ |
| $\dot{q}$ | heating rate, $Btu/ft^2\text{-}sec$ |
| $R$ | universal gas constant, 1545.32 $ft\text{-}lb_f/lb\ mol\ ^oR$ |
| $\mathcal{R}$ | universal gas constant, 1.1038 $cal/mol\ ^oR$ |
| $S$ | surface distance measured from hemisphere-cone tangent point (fig. 2(a)) |
| $t$ | time, sec |
| $T$ | temperature, $^oR$ |
| $V$ | speed, ft/sec |
| $W$ | weight, $lb_f$ |
| $x$ | distance measured from interface, ft (see fig. 4) |

| | |
|---|---|
| $\nabla$ | vector differential operator |
| Z | distance defined in figure 2(a) |
| $\delta_c$ | char thickness, ft |
| $\rho$ | mass density, $lb_m/ft^3$ |
| $\bar{\rho}$ | apparent density, $lb_m/ft^3$ |
| $\mu$ | viscosity, $lb_f$-sec/$ft^2$ |

Subscripts:

| | |
|---|---|
| aw | adiabatic wall |
| c | char |
| g | gases |
| i | interface |
| o | virgin material |
| P | plastic |
| TOT | total |
| w | wall |

## VII. FULL-SCALE MATERIAL TESTS

Since spallation appears to be a phenomenon which takes place primarily on large models (as opposed to arc jet models which are normally 1 to 3 inches in diameter), there are few ground facilities in which it can be observed. One such facility is the General Electric Company's Malta Test Station at Malta, N.Y. The Pit 4 facility at Malta consists of a 26,000 pound thrust rocket engine which has a shockless flow nozzle with an exit diameter of 15 inches. The heat shield model is mounted on a water-cooled model holder which holds the model in a vertical position. The engine is mounted in a gimbal arrangement which allows the test conductor to initiate and terminate engine ignition and shutdown in a "model off" position.

Nominal run conditions for the Pit 4 facility are as follows:

| | |
|---|---|
| Oxidizer/fuel ratio | 2.00 $lb_m/lb_m$ |
| Mass flow rate | 115 $lb_m$/sec |
| Combustion chamber pressure | 540 psia |
| Model stagnation pressure | 147 psia |
| Exit Mach number | 2.86 |
| Maximum stagnation temperature | 5300° F |

Figure 1 shows the Malta Pit 4 facility.

For the purpose of evaluating their relative performance, three carbon phenolic materials were tested in the Malta Pit 4 environment. The materials and their formulations are shown in Table I.

TABLE I.- COMPARISON OF MATERIALS

| Material | Reinforcement | Resin |
|---|---|---|
| NARMCO 4028 | 50 percent 1/4 inch carbon fibers | 50 percent phenolic |
| NARMCO 4088 | 64 percent 1/4 inch carbon fibers | 36 percent phenolic |
| NARMCO 4088-1 | 64 percent 1/4 inch carbon fibers | 36 percent filled phenolic (6-10 percent carbonaceous filler by wt) |

The materials described above were molded into conventional Pacemaker configuration heat shields (see fig. 2(a)). The Pacemaker configuration is a spherically blunted $10^{\circ}$ half-angle cone having an overall length of 13-1/2 inches and a base diameter of 10 inches.

The stagnation point heating rates on these models (calculated on the basis of measurements made previously at Malta) was 1700 $Btu/ft^2$-sec. The measured heating rate and pressure distributions on the conical portion of the models are shown in figure 2(b).

Figures 3(a) and 3(b) show the models under test. The pockmarked surface produced by the spallation process should be noted. Several observations may be made from these photographs, notably: (1) The spalled pieces of char leave the surface with considerable velocity; this enables them to travel normal to the flow for several inches before they are swept away. (2) The spallation is accompanied by the release of gases. (3) These gases appear to have high particle concentrations since they are visible in the photographs. Although not apparent from the photographs shown in figures 3(a) and 3(b), the author has made these additional observations based upon examination

of the films. (4) Spalled particles emanating from the hemispherical nose are smaller in size and occur more frequently than those emanating from the conical portion of the model. (5) There appears to be a "spallation front" which, although not always well defined, moves, with time, toward the base of the conical section. (6) Spallation can and does take place in areas which have previously undergone spalling. (7) There exists a pronounced difference between the rates at which the different materials spall. Most notably, NARMCO 4088-1 spalls approximately 1-1/2 times as often as does 4088, while the 4028 material spalled the least of the three materials tested.

## VIII. ANALYSIS

The photographs shown in figures 3(a) and 3(b) imply that spallation results from a buildup of internal pressure within the char; this culminates in failure of the char and release of the gases. According to reference 2 the pyrolysis of phenolics under extremes of pressure (to at least 60 atmospheres) occurs at essentially the same temperature as pyrolysis under atmospheric pressure. Assuming this is true, the problem is to determine the pressure drop across the char and identify those conditions which cause the pressure drop to increase to the point at which spallation occurs.

The momentum equation for flow through a porous matrix is given by Darcy's Law (ref. 3) which may be written as

$$\vec{V} = - \frac{k}{\mu} \left[ \nabla P - \left( \frac{\rho}{g_o} \right) \vec{g} \right] \qquad (1)$$

where $\vec{g}$ is the local gravitational vector (i.e. directed downward), $g_o$ is the reference gravitational constant, and $k$ is the permeability of the porous medium. The second term on the right hand side of equation (1) represents static head and, for the purposes of this paper, is negligible.

Reference 3 mentions the equation

$$\vec{V} = - \nabla \left( \frac{k}{\mu} P \right) + \frac{k}{\mu} \left( \frac{\rho}{g_o} \right) \vec{g}$$

as an alternate expression of Darcy's Law. This form, however, indicates that in the absence of a pressure gradient or static head, either a permeability gradient or a viscosity gradient is a sufficient

condition for flow. On an intuitive basis, this is not physically realistic. Furthermore, to the author's best knowledge, there is no experimental evidence reported in the literature to substantiate this form. With these arguments in mind, equation (1) has been used for this analysis.

At this point, we must refer to the one-dimensional model of the pyrolyzing ablator shown in figure 4. In this model of the ablator, there are three separate and distinct zones. The material in the first zone is virgin plastic. In the second zone, the virgin plastic is pyrolyzed. The third zone contains char and pyrolysis gases. The continuity equation for this model may be written as (ref. 3)

$$p \frac{\partial \rho}{\partial t} + \nabla \cdot \rho \vec{V} = 0 \tag{2}$$

where p, the porosity, is the ratio of the void volume in the char to the total volume of the char. By considering the virgin plastic as being composed of an irreducible, inert char skeleton filled with pyrolyzable material, we may write

$$\bar{\rho}_p = (1 - p)\, \rho_c + p\, \rho_g \tag{3}$$

where $\rho_c$ and $\rho_g$ are the mass densities of the irreducible char and the pyrolyzable material, respectively, and $\bar{\rho}_p$ is the apparent density of the plastic (i.e., instantaneous mass divided by initial volume). By taking the partial derivative of equation (3) with respect to time, we obtain

$$\frac{\partial \bar{\rho}_p}{\partial t} = p \frac{\partial \rho_g}{\partial t} \tag{4}$$

where the derivatives of the constant terms $p$ and $\rho_c$ are equal to zero. Upon substitution of equation (4) and insertion of the proper subscripts, equation (2) becomes

$$\left(\frac{\partial \bar{\rho}_p}{\partial t}\right) + \nabla \cdot \left(\rho \vec{V}\right)_g = 0. \tag{5}$$

Combining equations (1) and (5) and incorporating the equation of state

$$P = \rho \left(\frac{R}{M}\right) T \tag{6}$$

yields

$$\nabla \cdot \left(\frac{Mk}{\mu RT} PVP\right)_g = + \left(\frac{\partial \bar{\rho}_p}{\partial t}\right). \tag{7}$$

Friedman, in reference 3, presents a method which permits the pyrolysis reaction to be represented by the Arrhenius equation

$$- \frac{1}{W_o} \frac{dW}{dt} = A \left(\frac{W - W_c}{W_o}\right)^n e^{-\Delta E/RT} \tag{8}$$

where $W_o$ is the initial weight of virgin material, $W_c$ is the weight of char remaining after complete pyrolysis and $A$, $n$ and $\frac{\Delta E}{R}$ are experimentally determined constants.

Examination of equation (8) reveals that, since the rate of pyrolysis is dependent upon the instantaneous weight fraction of pyrolyzable material, pyrolysis will occur at some small finite rate in the zone shown in figure 4 as the char layer. In the presence of

a strong temperature gradient, however, the density profile will approximate that shown in figure 4 and result in a reasonably well defined interface with negligible pyrolysis rates in the char layer. In this analysis, we shall take the interface as the origin for the x coordinate, with x increasing in the direction of the virgin material as shown in figure 4. Equation (8) may be rewritten on a per unit initial volume basis as

$$-\frac{1}{\bar{\rho}_o}\frac{d\bar{\rho}}{dt} = A\left(\frac{\bar{\rho} - \bar{\rho}_c}{\bar{\rho}_o}\right)^n e^{-\Delta E/RT} \tag{9}$$

and incorporated into equation (7)

$$\nabla \cdot \left(\frac{\bar{M}k}{\mu RT} P \nabla P\right)_g = -\bar{\rho}_o A\left(\frac{\bar{\rho} - \rho_c}{\bar{\rho}_o}\right)^n e^{-\Delta E/RT}. \tag{10}$$

For the one-dimensional model, this can be rewritten

$$\frac{\bar{M}k}{\mu RT} P \frac{dP}{dx} = -\int_o^\infty \bar{\rho}_o A\left(\frac{\bar{\rho} - \bar{\rho}_c}{\bar{\rho}_o}\right)^n e^{-\Delta E/RT}\, dx = -\dot{m}_{g_i}. \tag{11}$$

As stated previously, it has been assumed that

$$\int_o^{-\delta_c} \bar{\rho}_o A\left(\frac{\bar{\rho} - \bar{\rho}_c}{\bar{\rho}_o}\right)^n e^{-\Delta E/RT}\, dx = \dot{m}_{g_{\delta_c}} - \dot{m}_{g_i} = 0. \tag{12}$$

If it is assumed that thermal gradients dominate in the char layer and diffusion within the char is neglected, then the temperature distribution (through the char layer) may be written as (see ref. 5)

$$T = T_i + \left[\frac{T_w - T_i}{H^*}\right]\left[(1 + H^*)^{-x/\delta_c} - 1\right] \tag{13}$$

where the surface of the char is at $x = -\delta_c$ and

$$H^* = \left(\frac{W_o - W_c}{W_o}\right) C_{P_{eff}} \frac{(T_w - T_i)}{H_p} \tag{14}$$

where $H_p$ is the heat of pyrolysis and $C_{P_{eff}}$ is the effective specific heat of the gas-char medium.

The mass flow rate of gases, $\dot{m}_{g_i}$, is related to the char thickness, $\delta_c$, by (ref. 4)

$$\dot{m}_{g_i} \delta_c = \left(\frac{K}{C_P}\right)_{eff} \ln (1 + H^*). \tag{15}$$

Now, rewriting equation (11) and substituting equation (15), yields

$$\int_{P_i}^{P_w} P \, dP = -\int_0^{-1} \left(\frac{k}{C_P}\right)_{eff} \ln (1 + H^*) \frac{\mu RT}{\bar{M}k} d\left(\frac{x}{\delta_c}\right) \tag{16}$$

which integrates to

$$P_i^2 = P_w^2 + 2 \left(\frac{k}{C_P}\right)_{eff} \ln (1 + H^*) \frac{R}{k} \int_0^{-1} \frac{\mu T}{\bar{M}} d\left(\frac{x}{\delta_c}\right). \tag{17}$$

For equation (17), the temperature, T, is given by equation (13). The quantity, $\mu/\bar{M}$, may be approximated from the method of reference 6 provided the constituent gases are known as a function of temperature. For the present study, the component gas fractions were obtained from an equilibrium chemistry program (ref. 7) based upon the empirical chemical formula of the NARMCO 4028 ablator.

Equation (17) was integrated using a digital computer, for five different combinations of assumed wall and interface temperatures. The results, plotted in figure 5, show the following: (1) a favorable

pressure gradient exists at all points in the char layer; (2) interface temperatures have little effect on the pressure at the interface; and, (3) the internal pressure increases with increasing wall temperatures.

The effect of increasing temperature, however, is not sufficient to account for the spallation phenomenon since, in ground tests, temperatures equilibrated rapidly while the "spalling front" moved, with time, down the length of the test cones. Furthermore, the effect of large wall temperature changes ($3500^{\circ}$-$5000^{\circ}$ R) does not substantially increase pressure. A reexamination of equation (17) shows that the only other means of producing large internal pressures is somehow to vary the permeability. Figure 6 presents the internal pressure as a function of char permeability. From this figure it is apparent that for a sufficiently low permeability, the char can spall regardless of wall or interface temperature.

Consider the following hypothesis: as pyrolysis occurs, small particles of carbon are carried out of the reaction zone by the escaping gases. These particles, in traveling through the porous char matrix, become entrapped, causing the permeability of the char to decrease with time. Since the rate of gas production is a function of heating rate, it may be expected that the rate of entrapment of particles will also be a function of the heating rate.

## IX. COMPARISON OF HYPOTHESIS WITH OBSERVATIONS

The preceeding hypothesis, if true, must explain the observations described in the section on Full Scale Model Tests. Observation (3) indicated that the pyrolysis gases at the interface did, indeed, have high particle concentrations. Observation (4) may be attributed to the very high heating rates experienced on the hemisphere. The high heating rates cause high blowing rates and rapid blocking; this causes the char to spall before it becomes very thick. Since heating rates are higher on the hemisphere than on the conical section, spalling occurs more frequently there. The "spalling front", noted in observation (5), can be explained as a line of constant permeability where permeability is given by an expression such as

$$k = k_o - \int_0^t f(\dot{m})\, dt$$

The movement of the "spalling front" is, then, due to decreasing heating rates (with distance) and increasing time. Observation (6) serves to point out that spallation results from a continuous phenomenon, such as has been hypothesized, rather than a phenomenon associated with say the original condition of the ablator surface. Observation (7) adds real weight to the hypothesis. Note that NARMCO 4088-1 differs from 4088 only in that it has a filled resin (i.e., the resin contains carbon or graphite particles). The filler particles at the time of pyrolysis have little structural or chemical affinity for the char forming about them; and under the hypothesis they act as

built-in contaminants which block the char. The high spalling rates, characteristic of NARMCO 4088-1, thus, bear out the hypothesis.

## X. PERMEABILITY TESTS

In order to establish that permeabilities are sufficiently low to cause high internal pressures and that the permeability of the char changes with time, measurements of char permeability were made. These tests employed half-inch diameter specimens of char, removed from each of the three nose cones. Char specimens were taken at varying distances from the rear of the cone in order to determine whether a variation of permeability with distance existed. The apparatus used to measure permeability is shown in figure 7.

In practice, use of the permeability test apparatus is quite simple. The sample to be tested is positioned at the outlet of the high pressure chamber. Air, at a controlled pressure, undergoes a pressure drop in passing through the specimen and another pressure drop in passing through the flow meter and out to the atmosphere. Prior to testing, the pressure drop across the flowmeter is measured as a function of flow rate. These data are then used to determine the downstream pressures in subseqent tests. The permeability measurements are made by varying the upstream (high) pressure from 0 to 100 psig in increments of 5 and 10 psi and recording the flow rate for each pressure. Upstream and downstream temperatures were also measured but the differences proved to be insignificant ($2^{\circ}$ to $3^{\circ}$ F).

Darcy's law (in the form of eq. 11) may be integrated at constant temperature and written as

$$\frac{\dot{m}_g}{P_{avg}} = \frac{k\bar{M}}{\tau\mu RT}\Delta P$$

where $\tau$ is the char thickness. Plotting the quantity $\frac{\dot{m}}{P_{avg}}$ as a function of $\Delta P$ provides a curve whose slope is $\frac{\bar{M}k}{\tau\mu RT}$. Since "slip flow" has been found to occur at low pressure gradients, the asymptotic limit of the slope should be used to determine permeability. A typical plot of permeabllity test data is shown in figure 8.

Figures 9-11 show the measured permeabilities as a function of distance from the rear surface of the cone. On each figure the approximate location of the "spalling front" is noted. Since the char in spalled areas is too thin to be tested, the specimens taken from locations forward of the "spalling front" were taken from unspalled areas.

In the areas aft of the "spalling front", the measured permeabilities all show a pronounced trend. The permeability can be seen to drop, very sharply, as the "spalling front" is approached. All specimens removed from locations forward of the "spalling front" exhibit higher permeabilities than would be expected from an extrapolation of the data trend aft of the front. This higher permeability, in fact, explains why they did not spall. The data, however, do not indicate why these locations had such high permeabilities. A close examination of the nose cones in the areas from which these specimens were taken revealed many minute cracks in the char. It would appear that these cracks provided the pyrolysis gases a low pressure drop path to the surface and thereby, retarding the clogging process locally.

It is interesting to note that upon reexamining the 3500° R curve of figure 6 one finds that these materials develop internal pressures of 1000 to 3000 psi before spalling.

Thus, having established that the spalling is caused by occlusion of the char and a resultant pressure buildup, the following inference can be made: (1) At least in high heating rate areas, the occlusion of the char should produce a noticeable increase in surface temperature, locally. Since the reduction in permeability causes a reduction in flow rate of the pyrolysis gases, the amount of heat blocked by transpiration of these gases will be reduced. This reduction in heat blockage will result in higher local net heating rates and a consequent increase in surface temperature. Having made this inference, the films were reexamined. Figure 12 shows this phenomenon and add, further, to the evidence indicating occlusion of the char with time. (2) Control of the char permeability will alleviate spalling. The molding process used to fabricate the Malta test nose cones produced a preferred fiber orientation. In the as-molded state, the majority of fibers lie in planes parallel to the local surface. This fiber arrangement produces the minimum permeability configuration. If, instead, the fibers were oriented so that they lay in planes normal to the surface a dual benefit should accrue. First, this fiber arrangement is conducive to higher permeabilities, and second, the resultant char is less resistant to cracking and, hence, has a greater ability to relieve internal pressures. By molding a cylindrical billet and then machining a nosecap from the billet, it is possible to get this selective orientation. Two different nosecaps with fibers oriented primarily in planes perpendicular to the axis of rotation have been tested, one at Malta and one in flight on the Pacemaker vehicle. Both nosecaps

show spalling in the areas where the fibers are parallel to the surface, but none in those areas where the fibers are nearly normal to the surface. This technique, then, has provided at least a partial solution to the spallation problem.

## XI. CONCLUSIONS

The foregoing analysis has resulted in the following conclusions:

1. The spallation of the carbon phenolic materials, as witnessed in the Malta Pit 4 tests, results from internal pressure buildup within the char layer.

2. The pressure increase within the char is caused by contamination of the porous char which, in turn, causes a decrease in permeability and a consequent increase in the pressure drop across the char layer.

3. The spallation process can be alleviated by selectively orienting the reinforcing fibers so that they are alined in planes normal to the local surface.

4. The fiber orientation most conductive to spalling is that which orients the fibers so that they lie in the plane of the surface. Molding processes appear to produce this type of orientation.

## XII. ACKNOWLEDGMENT

The author wishes to express his appreciation to the following people for their considerable assistance in the preparation of this thesis: , who programed the equations used; to and , who permitted the author to use their permeability test apparatus and provided both advice and encouragement; and to , the author's thesis advisor, whose understanding and encouragement provided the author with the necessary impetus to complete this project.

## XIII. REFERENCES

1. Allen, H. Julian; Seiff, Alvin; and Winovich, Warren: Aerodynamic Heating of Conical Entry Vehicles at Speeds in Excess of Earth Parabolic Speed. NASA TR R-185, 1963.

2. Madorsky, Smauel L.: Thermal Degradation of Organic Polymers. Interscience Publishers, 1964.

3. Scheidegger, Adrian E.: The Physics of Flow Through Porous Media. Rev. ed., The Macmillian Company, 1960.

4. Friedman, Henry L.: Kinetics of Thermal Degradation of Char Forming Plastics from Thermogravimetry. Application to a Phenolic Plastic. Journal of Polymer Science: Part C, No. 6, pp. 183-195.

5. Scala, Sinclaire M.; and Gilbert, Leon M.: Thermal Degradation of a Char-Forming Plastic During Hypersonic Flight. ARS Journal, June 1962, pp. 917-924.

6. Svehla, Roger A.: Estimated Viscosities and Thermal Conductivities of Gases at High Temperature. NASA TR R-132, 1962.

7. Zeleznik, Frank J.; and Gordon, Sanford: A general IBM 704 or 7090 Computer Program for Computation of Chemical Equilibrium Composition, Rocket Performance and Chapman - Jouquet Detonations. NASA TN D-1454.

**The vita has been removed from the scanned document**

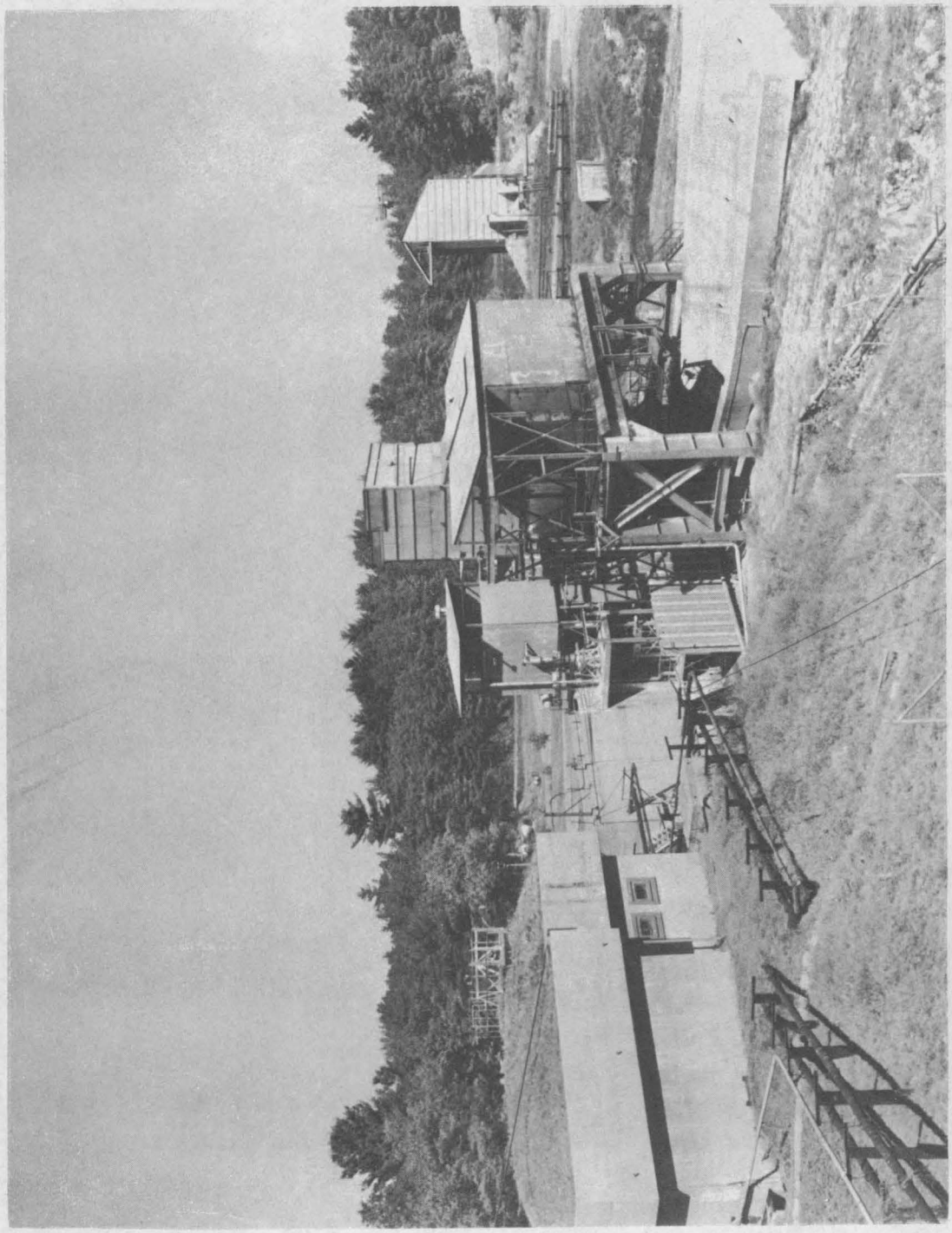

Figure 1.- Malta test facility - pit 4.

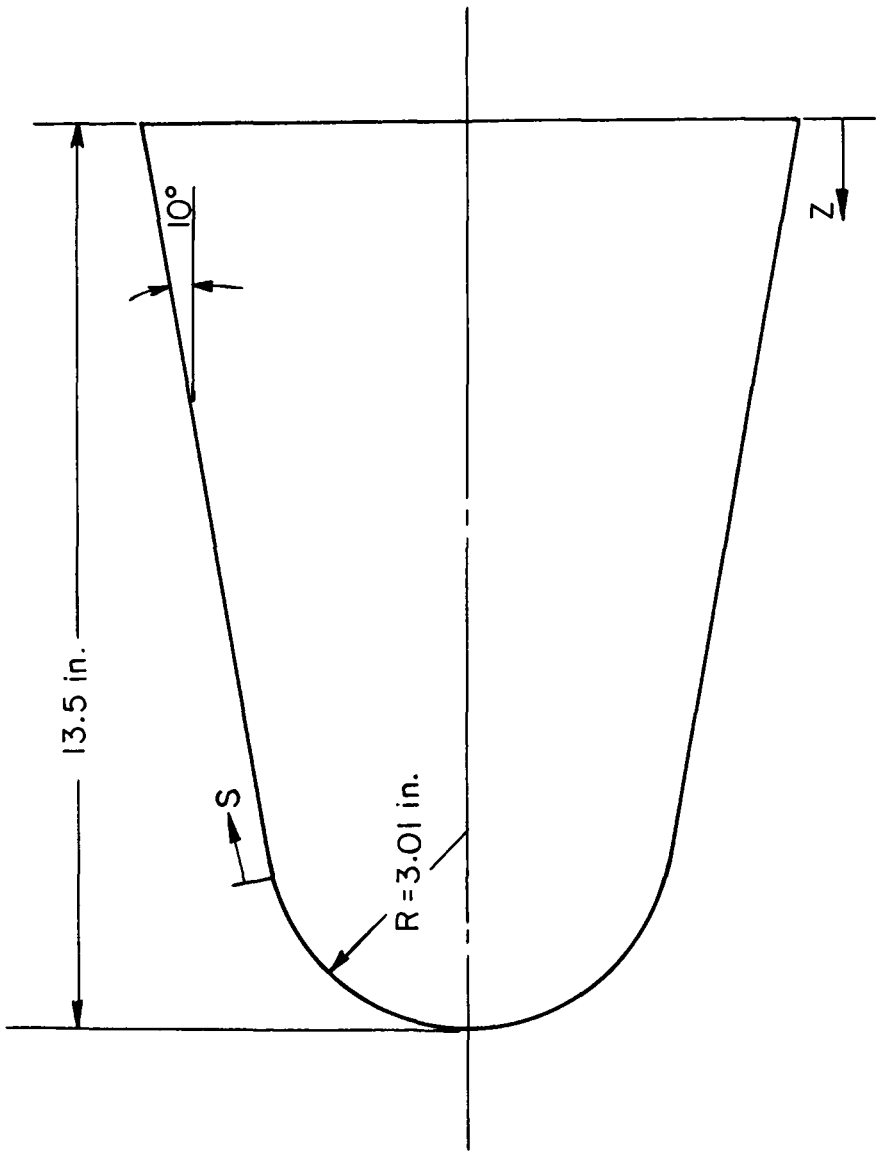


(a) Test model configuration.

Figure 2.- Full-scale test arrangement.

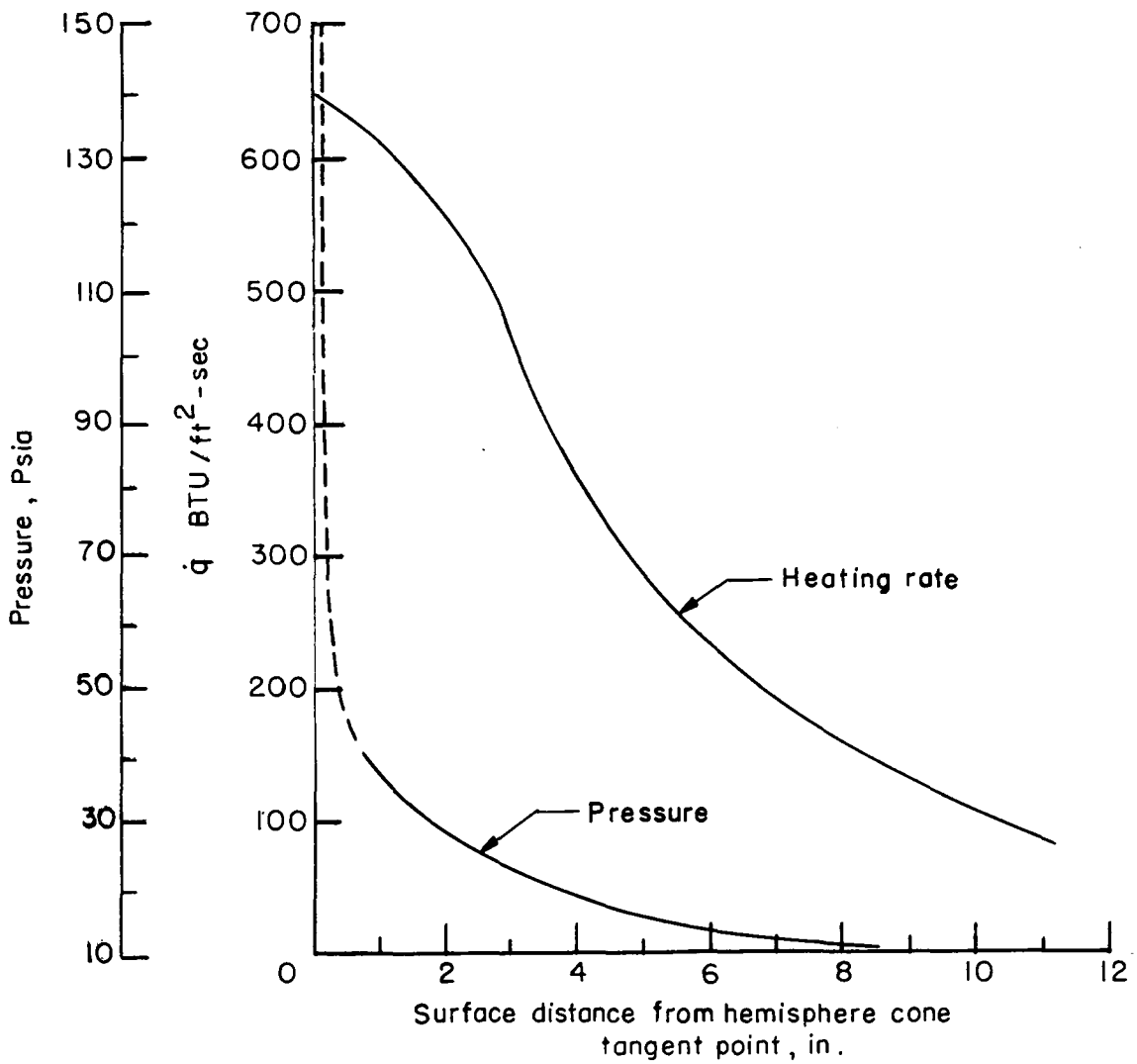


(b) Test conditions.

Figure 2.- Concluded.

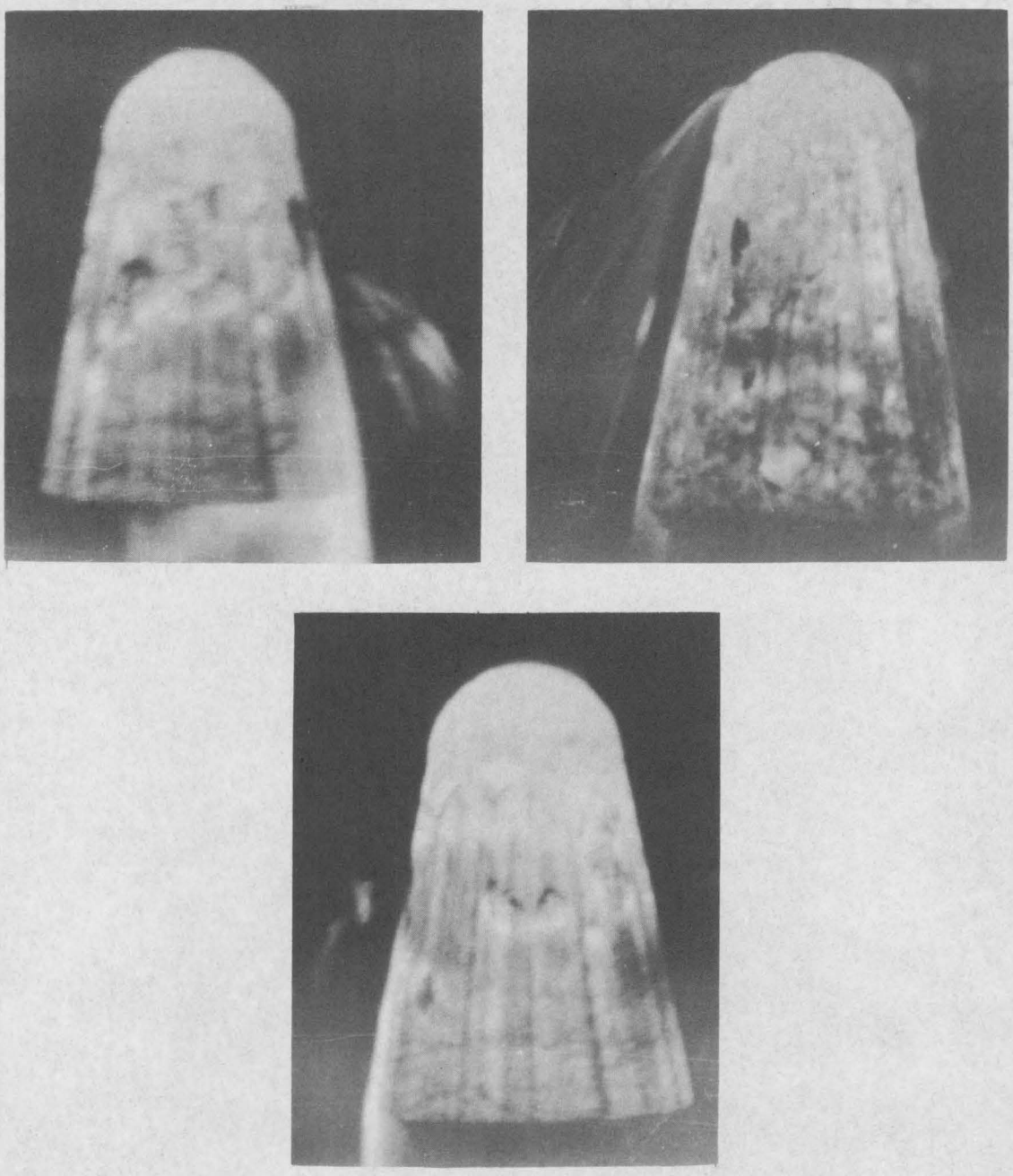

(a) Particles.

Figure 3.- Models under test.

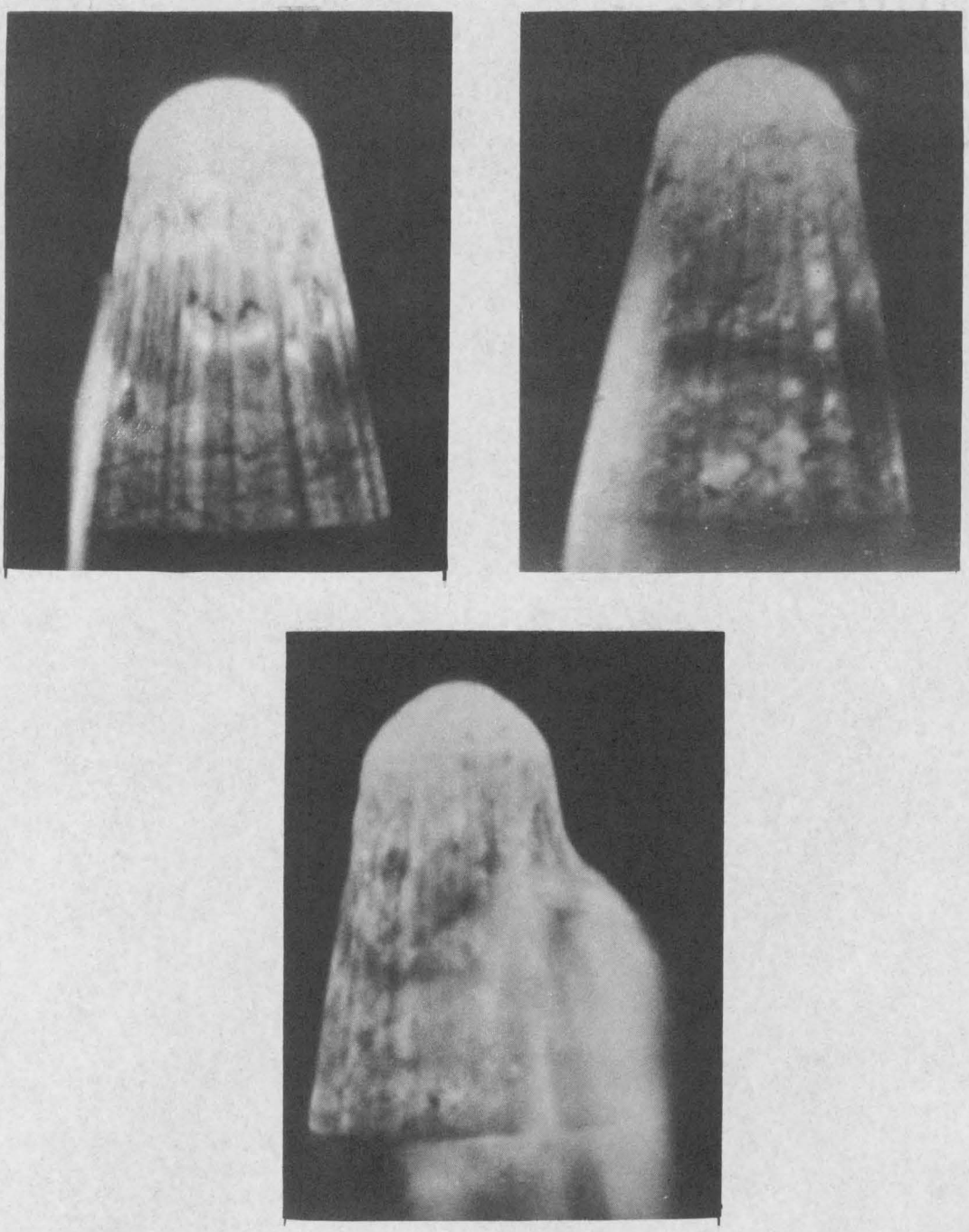

(b) Gases.

Figure 3.- Concluded.

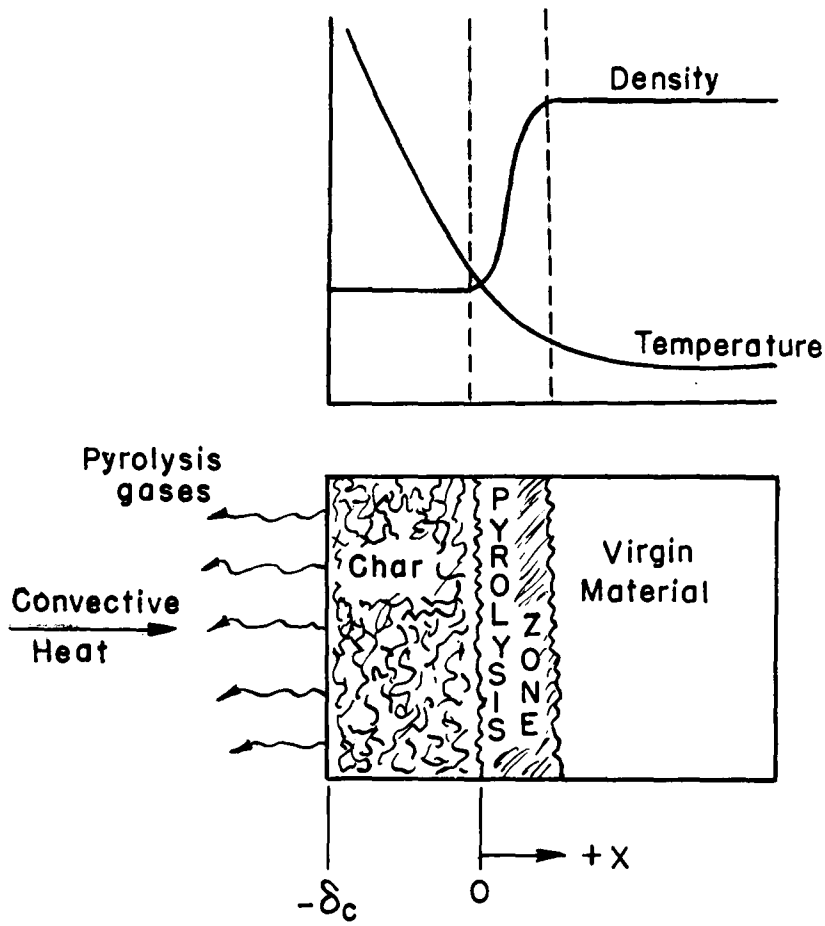


Figure 4.- One-dimensional model of ablator.

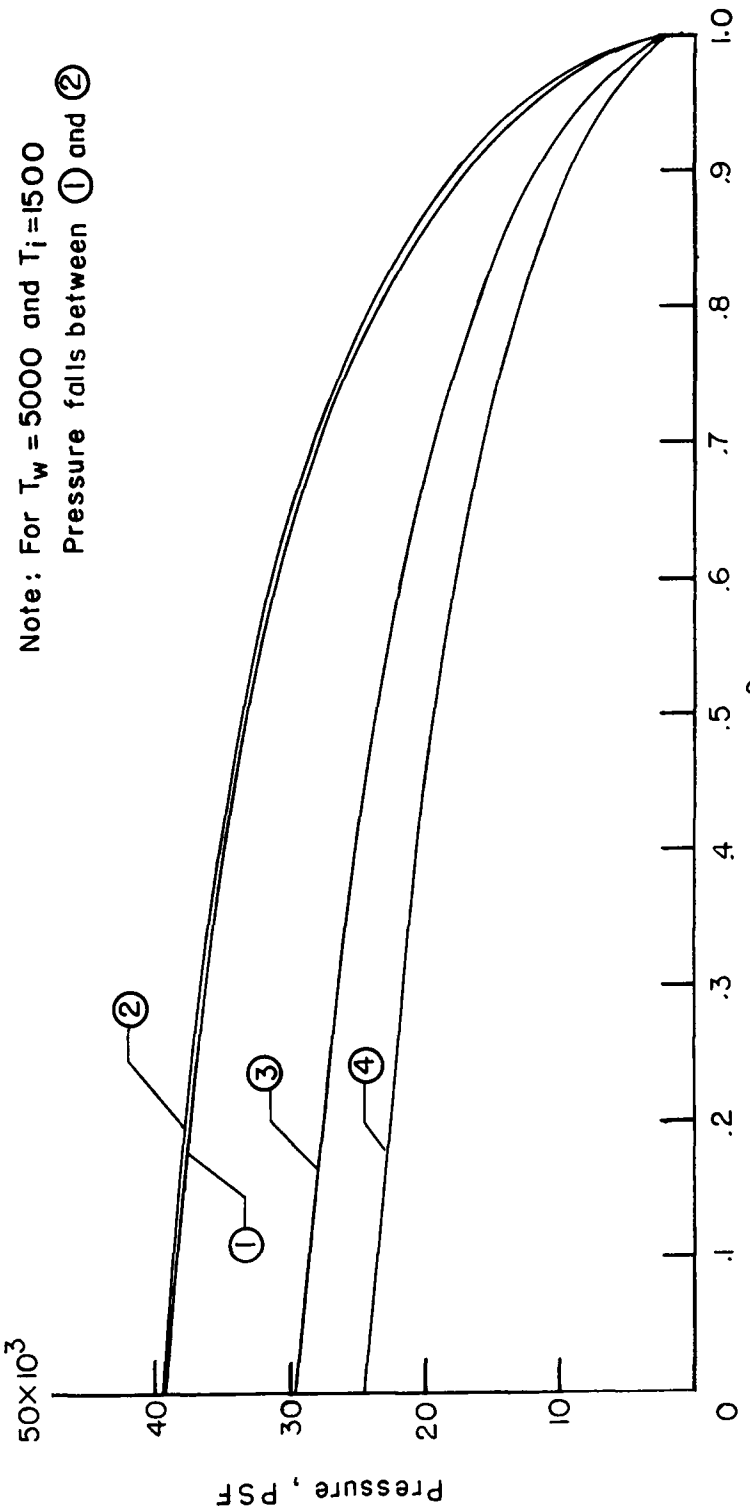


Figure 5.- Internal pressure distribution.

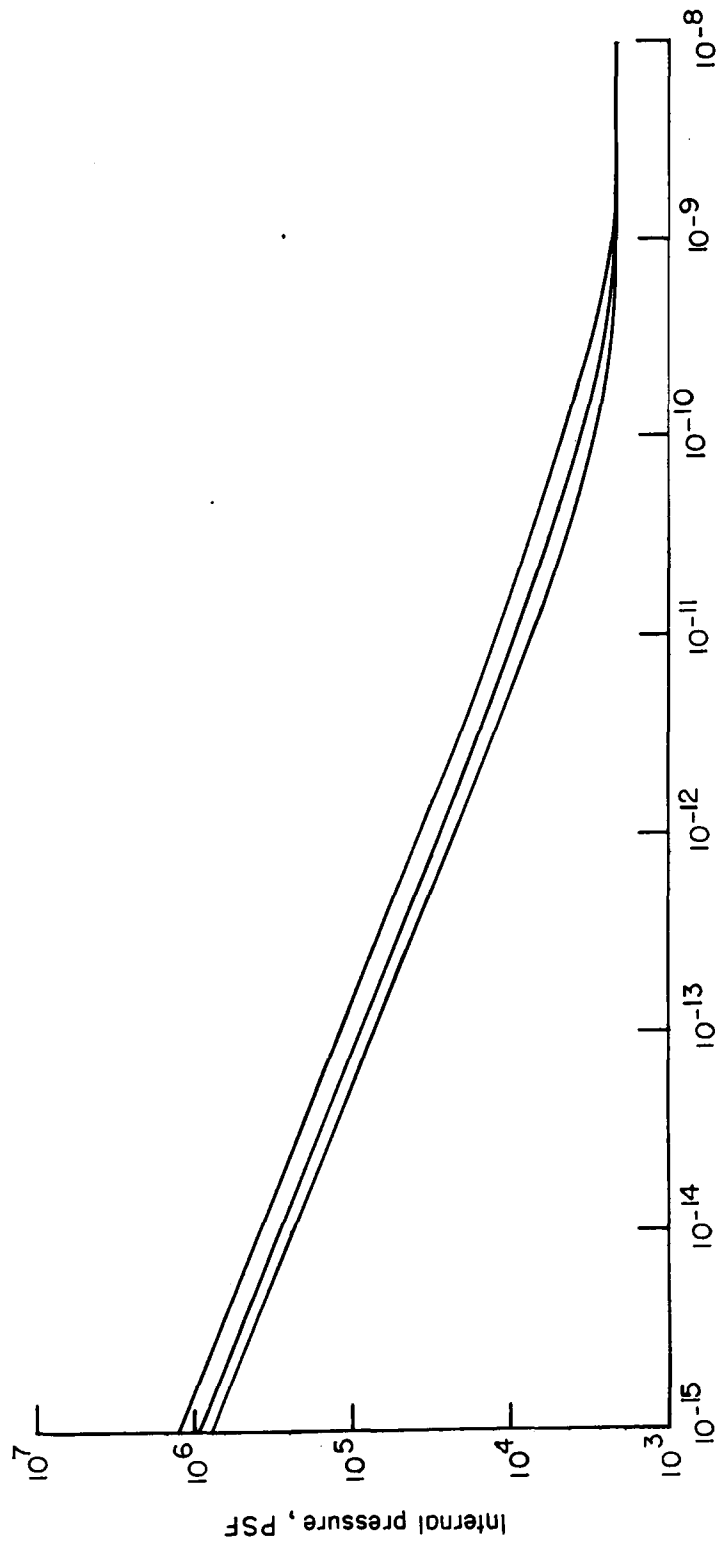


Figure 6.- Pressure dependence upon permeability.

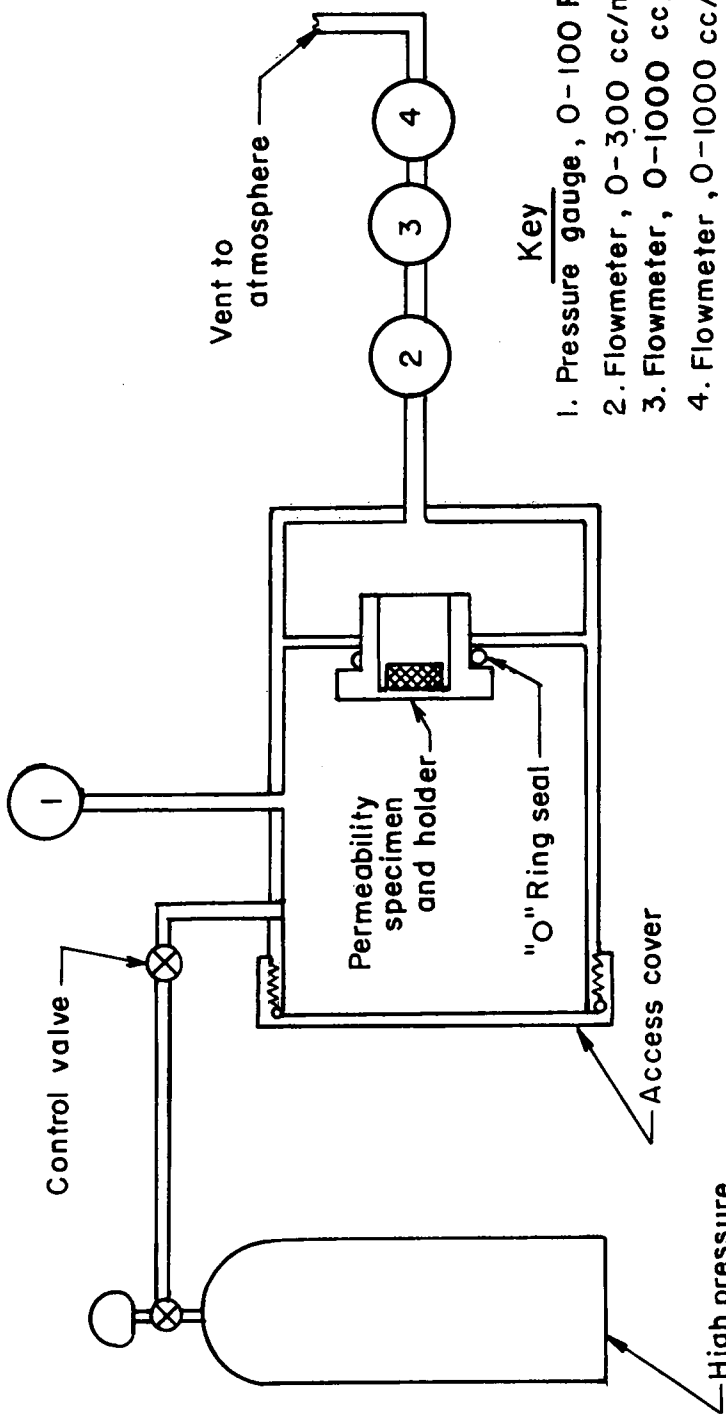


Figure 7.- Permeability test apparatus.

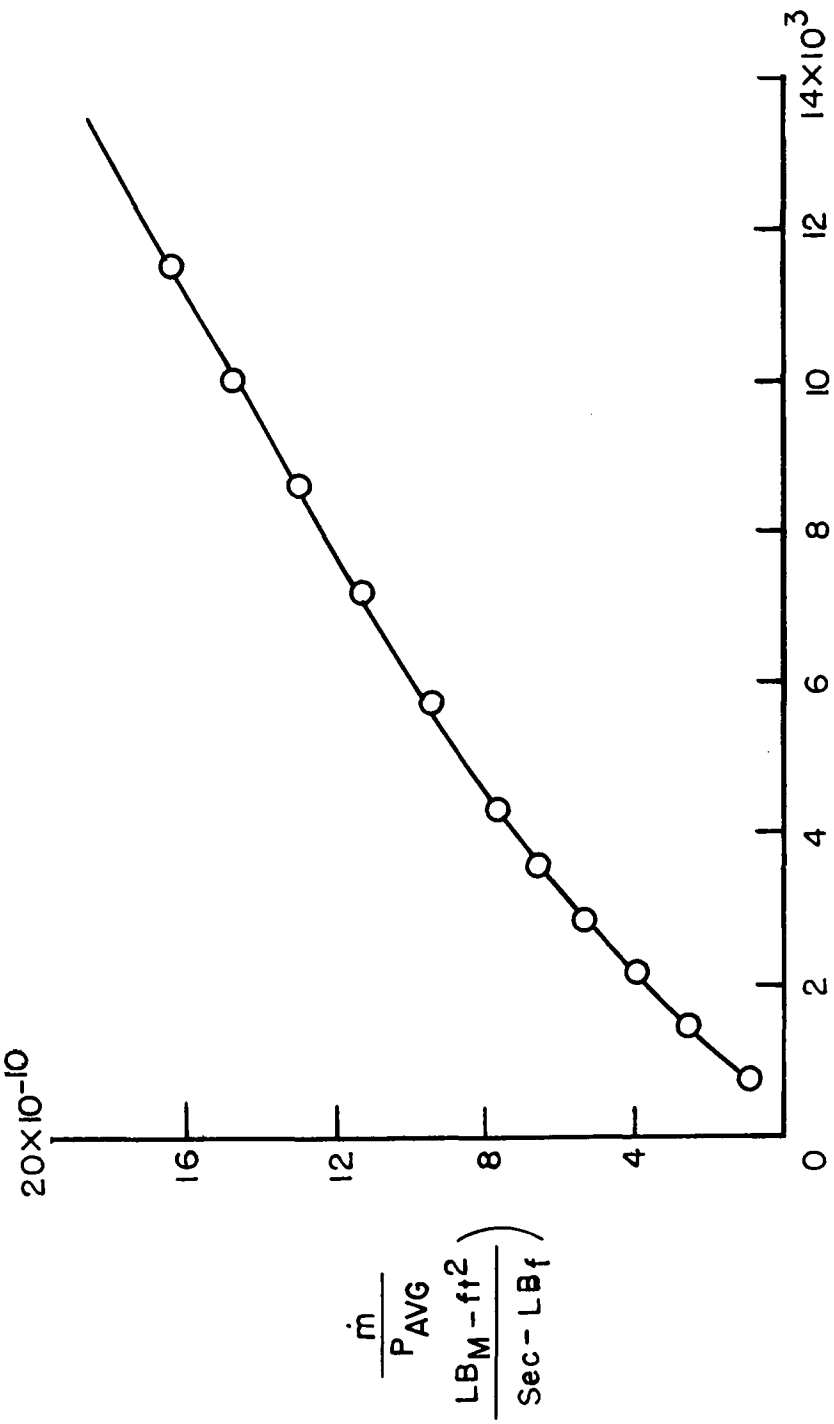


Figure 8.- Typical test data.

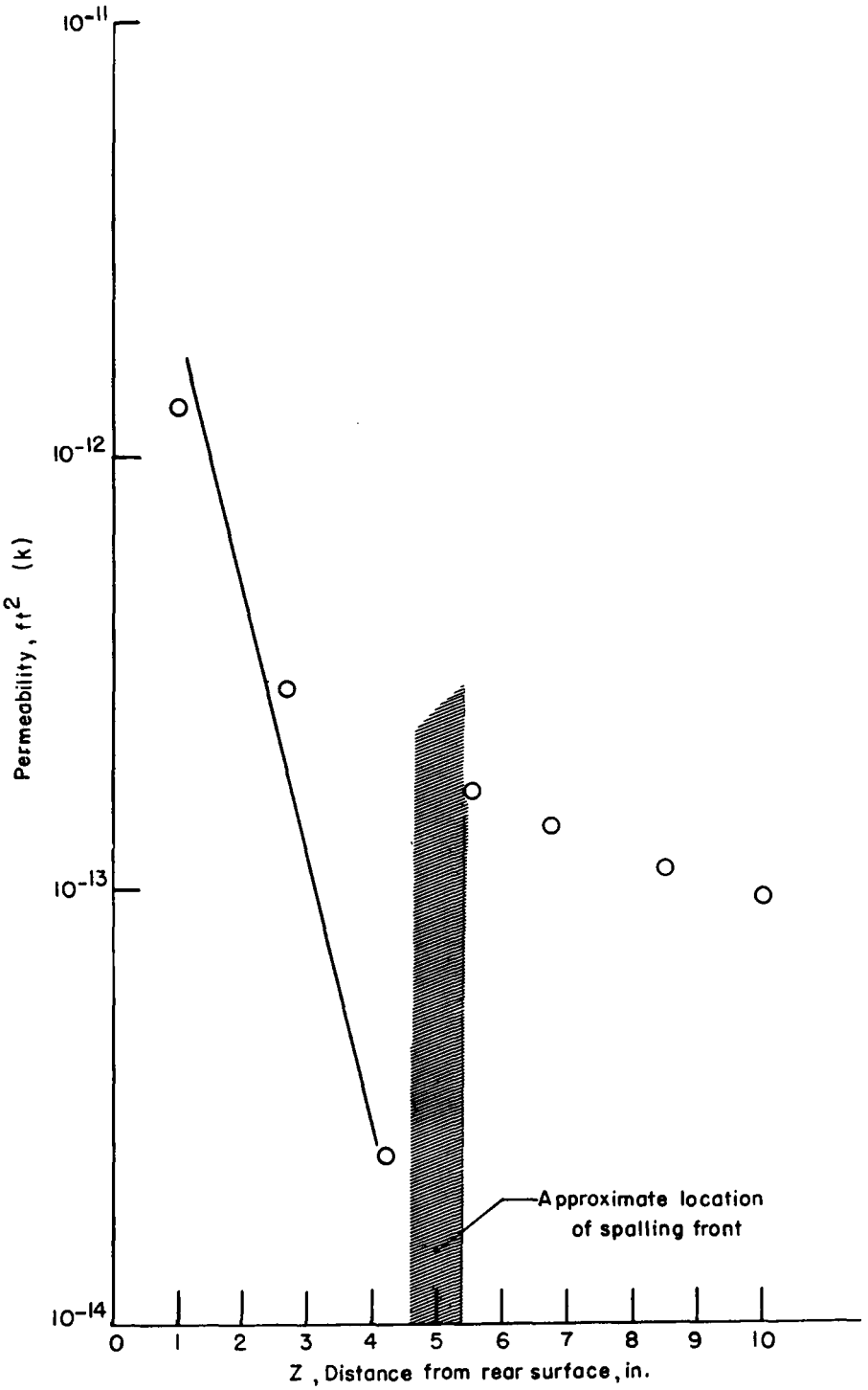


Figure 9.- Permeability measurements NARMCO 4028.

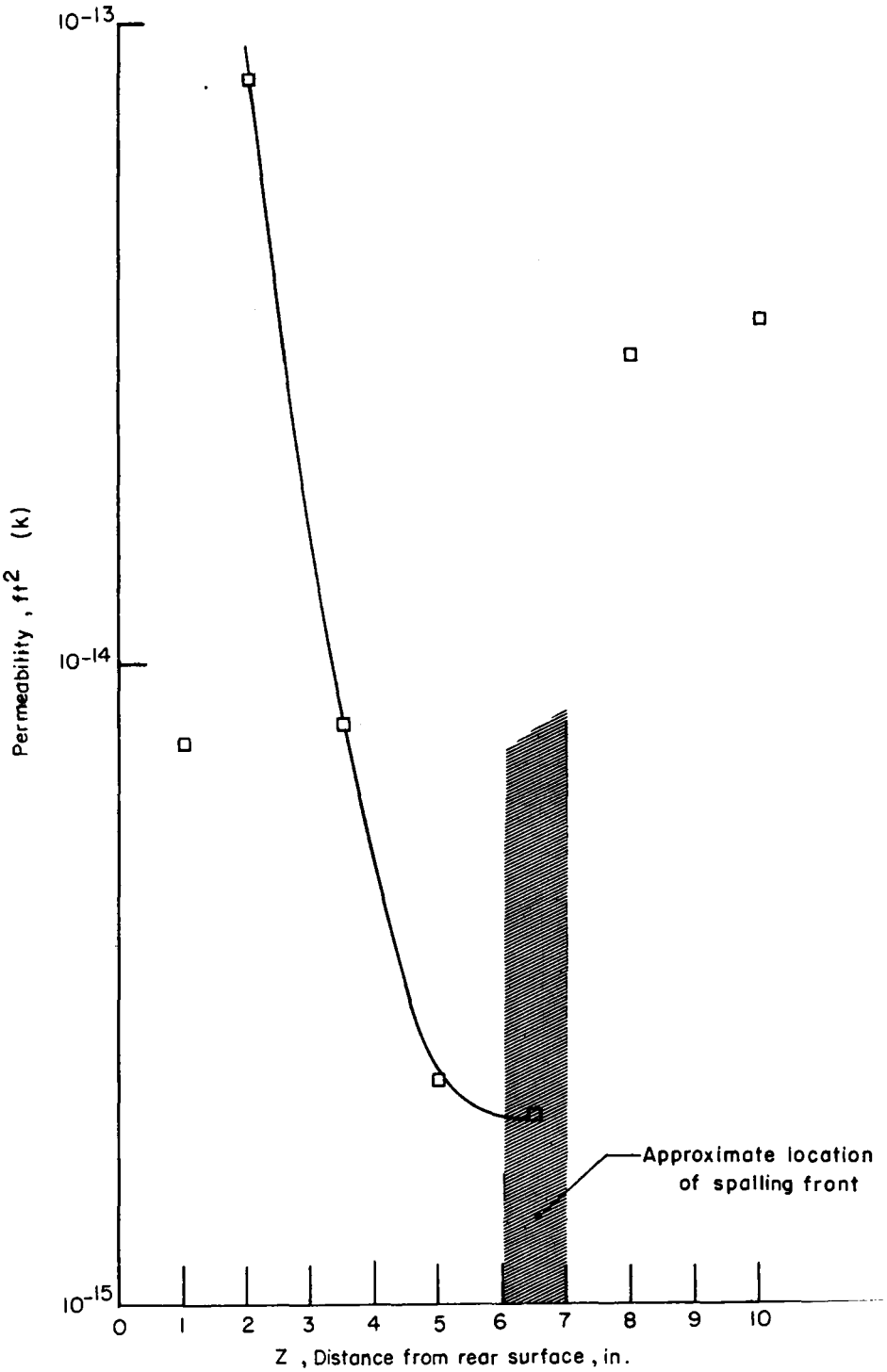


Figure 10.- Permeability measurements NARMCO 4088.

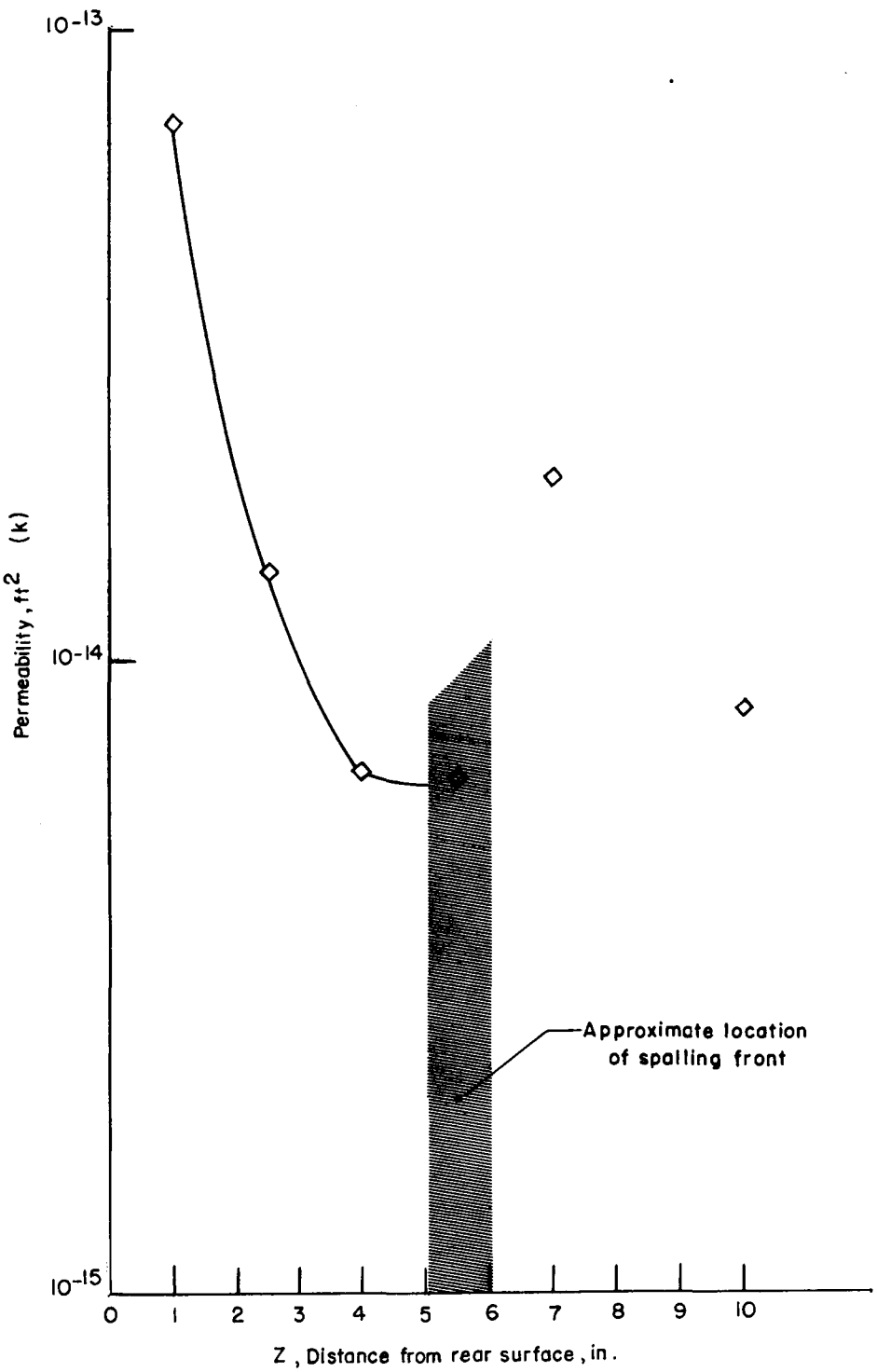


Figure 11.- Permeability measurements NARMCO 4088-1.

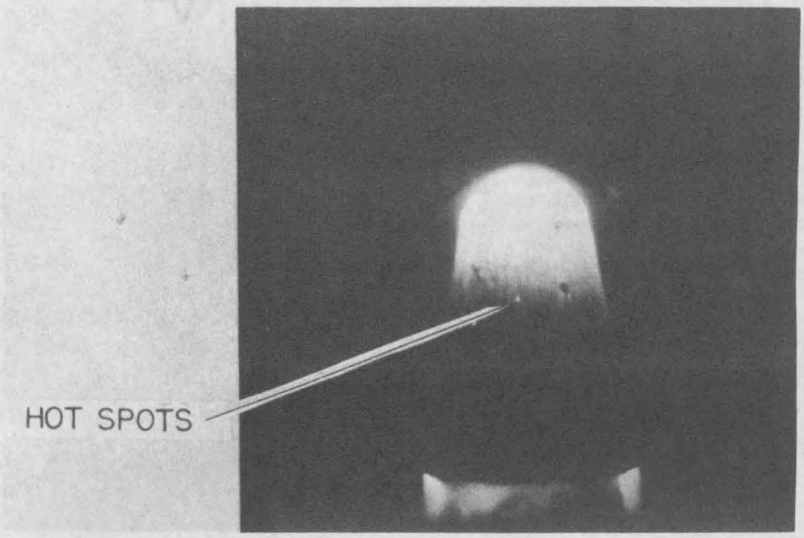


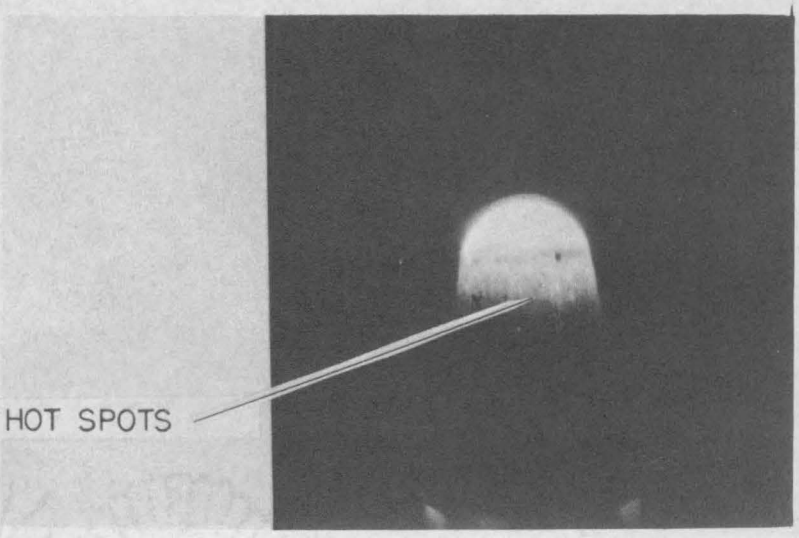


Figure 12.- Hot spots resulting from blockage of transpiration gases.

# AN ANALYSIS OF THE SPALLATION OF CRABON PHENOLIC ABLATORS

By

Brian J. O'Hare

## ABSTRACT

The phenomenon of spallation, a process by which pieces of char "pop off" a heat shield, has been investigated as it occurs in carbon-reinforced phenolic ablators. Spallation is shown to be the result of a pressure buildup within the char. This pressure increase results from occlusion of the char and the consequent blockage of flow. By selective fiber orientation, the spallation process can be alleviated.